JOINT DYNAMICS OF FLUID AND STRUCTURE

Janez Gale, Iztok Tiselj

Jožef Stefan Institute
1000 Ljubljana, Jamova 39, Slovenia

Janez.Gale@ijs.si (Janez Gale)

Abstract

The joint dynamics of fluid and structure, also known as Fluid-Structure Interaction, considered in this study, refers to piping systems conveying fluid transients. The question what is the influence of the flexible piping system on a fluid transient is not fully answered yet although it has been theoretically and experimentally widely investigated. This question is especially important for industries where transient appearance is feasible or even anticipated during the normal operation of the particular system and where failure of the piping system can cause severe accidents, releases of rare or dangerous substances or jeopardize human lives. The objective of this paper is to report new approach to simulations of the Fluid-Structure Interaction in piping systems filled with single-phase fluid (water). The basic four equations model for description of the two-way interaction between the fast transient in the fluid and axial movement of the pipe, are improved with additional four Timoshenko beam equations for description of the flexural motion (rotation and deflection). The proposed model enables simulations of any arbitrarily shaped piping system in plane. The considered coupling procedure enables full two-way Poisson and junction coupling of the fluid and structure i.e. it is possible to analyze and evaluate influence of the flexible pipe on the single-phase fluid transient. Special attention is given to applied high resolution characteristic upwind numerical method, which is based on Godunov's method. The proposed method is verified with single-phase rod impact benchmark experiment.

Keywords: Fluid-Structure Interaction, Transient Structural and Fluid Dynamics, Numerical Modeling, Nonlinear System.

Presenting Author's biography

Janez Gale. Bachelor of Science in hydrology, 2001 (Faculty of Civil and Geodetic Engineering, University of Ljubljana). Since December 2001 employed at Jožef Stefan Institute – Reactor Engineering Division, involved in research of Fluid-Structure Interaction, fast transients and fluid thermal and hydro dynamics in piping systems of nuclear power plants (thermal and mechanical relaxation), metastable states, water hammer. Ph.D student since 2003 (Two-phase flow transients and interactions with piping systems).

1 General

Joint dynamics of the fluid and the structure, also known as Fluid-Structure Interaction (FSI), has been a very 'hot' topic in the last few decades as efficiency and safe operation of the piping systems became more important. The FSI is defined as exchange of energy between the moving fluid and flexible structure. The FSI is very general term covering numerous phenomena from the field of aeronautics, civil engineering, energy production, chemical and oil industry, and many more sciences like for instance music instruments or hemodynamics in the human body. The present paper is focused on the slender hollow piping structures with circular cross-section conveying single-phase transient flow in the fluid. Although FSI is less fatal in steady state flow, mainly because flutter and vibrations can be detected and limited with additional corrective actions, the detrimental effects of the FSI can become very important during the unanticipated transient conditions. The transient pipe flow can emerge due to the inappropriate valve operation, at stop or start-up of the pumps, if cold water is injected into steam, during the system temperature changes, during the rapid pressure or velocity changes in the fluid, especially accidental.

It is estimated that 98% of piping systems are not subjected to significant influence of the fast transient in the fluid; however, Professor Wylie [1] was concerned with the fact that there is no reliable criterion, which would signify whether the FSI is relevant for the particular piping system. Therefore, in order to avoid significant damage or fatalities, Wylie recommends FSI analysis for all piping systems. The first who proposed reliable criterion for inspection of the FSI in pipes during the fluid transient were Lavooij and Tijsseling [2]. The proposed criterion was validated for inspection of the FSI in a single elbow piping system geometry. The criterion is based upon natural period of the structure, valve closure time and period of the water hammer waves. Casadei [3] indicated qualitative criterion based upon engineering judgement. Casadei always recommends FSI analysis in flexible piping systems (lower number of supports, thin walls) with sharp pressure waves in an incompressible single-phase liquid. The author's experience with two-phase flow modeling [4] shows that maximal pressure in the fluid predicted with classical Joukowsky theory for single-phase flow [5] can be exceeded by as much as 60%, thus we believe it is possible that the effects of the two-phase flow can increase the detrimental effects of the FSI. However, with appropriate FSI analysis followed by appropriate design and definition of the optimal operating procedures, it is possible to control the energy transfer between the fluid and the structure and thus: (i) to control the maximal pressures and stresses in the system, (ii) to prevent fatigue or the ultimate failure of the piping system and (iii) to prevent fatigue or the ultimate failure of the support/restraint system.

The most important literature dealing with the FSI in piping systems is that of Païdoussis [6] who performed exhaustive summary over the FSI field with emphasize on a steady state flow induced flutter, vibration and resonance. Wiggert and Tijsseling [1,7,8] performed several systematic reviews of the experimental and theoretical FSI research of the transient pipe flow. One of the important differences between the FSI models described by Wiggert and Tijsseling is in the number of equations i.e. in the number of the tracked stress and pressure waves that travel along the pipe or water and interact with each other. According to the interactions between the waves in piping systems, it is possible to distinguish distributed Poisson and friction coupling, and the local junction coupling [1]. The Poisson coupling describes interaction of pressure waves in the fluid with axial and radial waves in the structure (pipe breathing), the junction coupling describes interaction of waves at geometric changes like elbows, cross-section changes, valves, junctions, pipe ends, etc., and finally the friction coupling describes forces initiated due to the difference between the fluid and the structure velocity. The friction coupling is usually negligible comparing to intensity of the junction and Poisson coupling. There have been several attempts to evaluate dynamic forces of the fluid on the structure known also as one-way coupling, but there are only a smaller number of them that takes into account also forces of the structure on the fluid. These methods are known as two-way coupling methods [1].

2 Mathematical system of equations

2.1 Eight-equation model

The mathematical model is similar to the PDEs system described by Valentin, Philips and Walker [9] who introduced four Timoshenko beam equations into classical four-equation model defined by Skalak [10]. Tijsseling, Vardy and Fan [11] presented the system of equations with identical convective part but different source terms. Their mathematical model enables simulations of the FSI in two straight sections with constant properties. The sections are connected with additional relations (boundary conditions). Hu and Philips [12] and De Jong [13] analyzed similar system to Tijsseling, Vardy and Fan [11] in the frequency domain. The system of eight 1st order linear PDEs enables two-way FSI coupling and takes into account Poisson and junction coupling mechanisms, while the friction coupling can be easily implemented. Among the several types of the waves that characterize FSI, the eight-equation model is able to describe axial, rotational and flexural stress waves in the pipe and pressure waves in the fluid. The piping system is considered as one-dimensional (pipe's internal radius << pipe's length). The cross-section is circular and not necessary uniform along the pipe. The applied source terms enable modeling of the planar arbitrarily shaped piping systems. The stress-strain relations are linear elastic in accordance with the Hooke's law. If the transient occurs and remains in an adiabatic single-phase liquid flow at the room temperature $T = 295\ K$, with pressure change within *1 and 40 bar*, then the fluid density alters for about 0,18 % and the corresponding speed of sound alters for about 0,44% (Fig. 1). Figure 2 shows that density change in single-phase conditions is almost diminutive, therefore, it is assumed that the density is constant. Figures 1 and 2 show that this assumption is correct but note that only a minor part of real transients occur in pure single-phase.

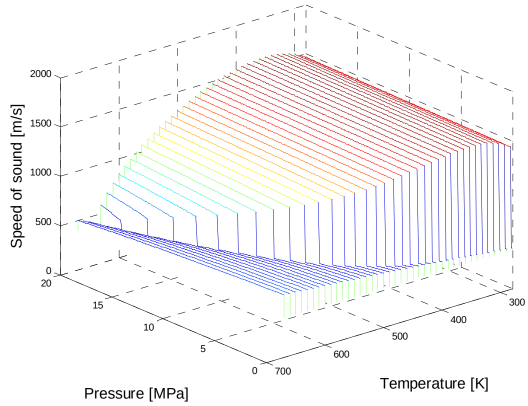

Fig. 1: Characteristic velocity of the pressure waves, i.e. the speed of sound in infinite fluid with sharp discontinuity at phase change [14].

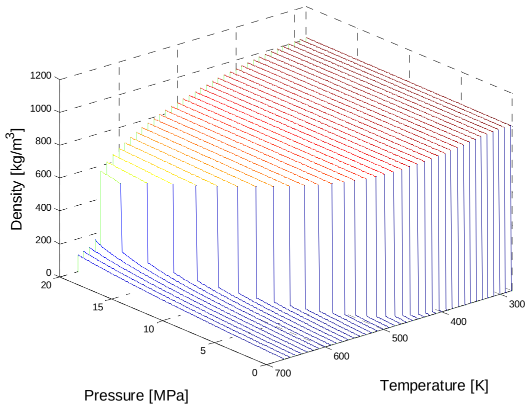

Fig. 2: Fluid density with sharp discontinuity at phase change [14].

The fluid part of the considered eight-equation model contains two 1D linear 1st order PDEs, which are energy conserving (no damping and friction), single-phase (no cavitation), valid for pressure waves with low frequency (long wavelength approximation). The momentum equation reads:

$$\rho_f \frac{\partial v}{\partial t} + \frac{\partial p}{\partial x} = 0 \tag{1}$$

where v stands for fluid velocity, p for fluid pressure, t stands for the time, x for the axial position and ρ_f for the (constant) fluid density. The continuity equation reads:

$$\frac{1}{K'}\frac{\partial p}{\partial t} + \frac{\partial v}{\partial x} - \frac{2\nu}{EA_t}\frac{\partial N_x}{\partial t} = \frac{u_y}{R_p} \tag{2}$$

where

$$\frac{1}{K'} = \frac{1}{K} + \frac{2R}{Ee}\left(1-\nu^2\right) \tag{3}$$

with N_x as axial force, u_y as lateral pipe velocity, R as the internal radius of the pipe, d as the pipe thickness, ν as the Poisson's ratio, E as the Young's elasticity modulus and K as the fluid bulk modulus.

Two equations are used for description of the propagation of the axial stress waves in the straight, thin-walled, linearly elastic pipe of circular cross-section. The 1D first order PDEs are derived from the axial wave equation for the pipe where the equation of motion is:

$$\frac{1}{EA_t}\frac{\partial N_x}{\partial t} - \frac{\partial u_x}{\partial x} - \frac{\nu R}{Ee}\frac{\partial p}{\partial t} = -\frac{u_y}{R_p} \tag{4}$$

with u_x as axial pipe velocity. The general constitutive equation governing axial stresses:

$$\rho_t A_t \frac{\partial u_x}{\partial t} - \frac{\partial N_x}{\partial x} = -\frac{Q_y}{R_p} \tag{5}$$

with Qy as shear force, and ρ_t as pipe wall density. Additional two generalized constitutive equations governing the transverse shear force and the bending moment are:

$$\frac{1}{kA_t G}\frac{\partial Q_y}{\partial t} - \frac{\partial u_y}{\partial x} = \frac{u_x}{R_p} - \varphi_z \tag{6}$$

$$\frac{1}{EI_t}\frac{\partial M_z}{\partial t} - \frac{\partial \varphi_z}{\partial x} = 0 \tag{7}$$

and two equations of motion:

$$\left(\rho_f A_f + \rho_t A_t\right)\frac{\partial u_y}{\partial t} - \frac{\partial Q_y}{\partial x} = \frac{N_x - pA_f}{R_p} \tag{8}$$

$$I_t \rho_t \frac{\partial \varphi_z}{\partial t} - \frac{\partial M_z}{\partial x} = Q_y \tag{9}$$

where M_z stands for bending moment, φ_z for rotational velocity of the pipe, A_t for the area of pipe's wall cross section and I_t for the moment of inertia. Eqs. 6-9 are also known as the Timoshenko's beam equations [15].

2.2 Vectorial form of the equations

The system of eight linear PDEs can be written in the following vectorial form:

$$\mathbf{A}\frac{\partial \vec{\psi}}{\partial t}+\mathbf{B}\frac{\partial \vec{\psi}}{\partial x}=\vec{S} \tag{10}$$

where all temporal and spatial derivatives are collected on the left hand side (convective terms) and all non-differential terms are collected on the right hand side (source terms). The vector $\vec{\psi}=\{v, p, u_x, N_x, u_y, Q_y, \varphi_z, M_z\}$ is a vector of eight basic independent variables. Matrices **A** and **B** are matrices of the system. The first two rows of this system belong to the continuity and the momentum balance equation of the fluid, the third and the fourth row to the wave equation of the axial motion of the structure and the last four rows to the Timoshenko's beam equations for the lateral and the rotational motion. The parameters of the matrices **A** and **B** could be assumed as constant with time and space (constant coefficient system). This is necessary for use of the Method of Characteristics and it is valid only for some certain problems where changes of the fluid properties or geometry are actually diminutive.

2.3 Characteristic form of equations

The vectorial form can be rearranged into:

$$\frac{\partial \vec{\psi}}{\partial t}+\mathbf{A}^{-1}\mathbf{B}\frac{\partial \vec{\psi}}{\partial x}-\mathbf{A}^{-1}\vec{S}=0 \tag{11}$$

and considering $\mathbf{A}^{-1}\mathbf{B}=\mathbf{C}=\mathbf{L}\boldsymbol{\Lambda}\mathbf{L}^{-1}$ and $\vec{R}=-\mathbf{A}^{-1}\vec{S}$ the characteristic form of the equations yields:

$$\frac{\partial \vec{\psi}}{\partial t}+\mathbf{L}\boldsymbol{\Lambda}\mathbf{L}^{-1}\frac{\partial \vec{\psi}}{\partial x}+\vec{R}=0 \tag{12}$$

The eight-equation system is **hyperbolic** because the Jacobian matrix $\mathbf{C}$ with dimension eight has eight real eigenvalues $\boldsymbol{\Lambda}$ and has a corresponding set of eight independent eigenvectors $\mathbf{L}$. The eight eigenvalues of the Jacobian matrix are actually characteristics, which represent speed of the eight distinct pressure or stress waves traveling inside the fluid and structure. The characteristic form of the equations represents the basis for the applied Godunov's numerical scheme. With additional matrix operations and introduction of the modified characteristic variables:

$$\delta\vec{\xi}=\mathbf{L}^{-1}\delta\vec{\psi}+\boldsymbol{\Lambda}^{-1}\mathbf{L}^{-1}\vec{R}\delta x \tag{13}$$

one can get very elegant modified characteristic form of the Eq. 10 that is used for evaluation of the flux (slope) limiters:

$$\frac{\partial \vec{\xi}}{\partial t}+\boldsymbol{\Lambda}\frac{\partial \vec{\xi}}{\partial x}=0 \tag{14}$$

2.4 Source terms

The vector $\vec{S}$ is vector of the source terms:

$$\vec{S}^T=\left\{\frac{u_y}{R_p},0,-\frac{Q_y}{R_p},-\frac{u_y}{R_p},\frac{N_x-pA_f}{R_p},\frac{u_x}{R_p}-\varphi_z,Q_y,0\right\} \tag{15}$$

The source term vector in this form enables junction coupling of the fluid transient and the axial movement with the lateral and the rotational movement for each section of the pipe where the pipe's curvature radius R_p is reasonable. For cases where pipe's curvature radius R_p approaches infinity (straight pipes), the vector of the source terms reduces to the source terms described by Tijsseling, Vardy and Fan [11]:

$$\vec{S}^T=\left\{0,0,0,0,0,-\varphi_z,Q_y,0\right\} \tag{16}$$

With this set of the source terms it is possible to simulate straight sections of the pipe connected by relatively short elbows.

2.5 Boundary conditions

For rod impact experiment described in Section 4, the following relations are used as boundary conditions of the computational domain (junction coupling included):

- Beginning: closed pipe, no support, rod impact in the axial direction of the pipe:

$$v=u_x\ ,\ N_x=A_f p+Y_{rod}\left(u_x-v_{0,rod}\right) \qquad Q_y=0\ ,\ M_z=0 \tag{17}$$

  where $Y_{rod}=A_{rod}\,(E_{rod}\,\rho_{rod})^{1/2}$ is admittance or impedance of the rod and $v_{0,rod}$ impact velocity of the rod [11].

- End: closed pipe, no support:

$$v=u_x\ ,\ A_f p=N_x\ ,\ Q_y=0\ ,\ M_z=0 \tag{18}$$

3 Numerical method

Typical numerical methods developed for linear conservation laws are valid for smooth solutions, but these methods are not sufficient for description of the multiple sharp pressure or stress waves that are traveling along the pipe during the transient pipe flow. It is known that first-order accurate numerical methods like Lax-Friedrichs or Upwind give smeared solutions near the wave, especially on coarse grids [16] that is known as numerical dissipation. The second-order accurate numerical methods like Lax-Wendroff or Beam-Warming do not suffer due to the numerical dissipation but give unstable solutions in the vicinity of the sharp waves. Oscillations are typical for all second-order accurate methods [17].

3.1 Characteristic upwind method

Characteristic upwind method is an advanced upwind first-order, explicit and 2-level numerical method for linear and nonlinear hyperbolic systems [16]. It is based on Godunov's methods, which enables appropriate splitting between the wave propagation to the left and to the right (superscripts – and +, respectively) and it thus enables proper handling for systems of equations where the waves propagate in both directions. The discretisation of the Eq. 14 yields:

$$\frac{\vec{\xi}_j^{n+1} - \vec{\xi}_j^n}{\Delta t} + \left(\mathbf{\Lambda}^+\right)_{j-1/2}^n \frac{\vec{\xi}_j^n - \vec{\xi}_{j-1}^n}{\Delta x} + \left(\mathbf{\Lambda}^-\right)_{j+1/2}^n \frac{\vec{\xi}_{j+1}^n - \vec{\xi}_j^n}{\Delta x} = 0 \tag{19}$$

where $\mathbf{\Lambda}^+ = diag\left(\lambda_1^+, ..., \lambda_8^+\right)$, $\mathbf{\Lambda}^- = diag\left(\lambda_1^-, ..., \lambda_8^-\right)$. Subscripts j and $j\pm 1$ denote grid points of the spatial discretisation that are located in the middle of each control volume and subscripts $j\pm 1/2$ denote values in the midpoint of two grid points. The Δx denotes distance between the two neighboring grid points, and the Δt denote time step interval between time levels n and $n+1$. The appropriate splitting between positive and negative waves is obtained by multiplication of the eigenvalues with correction factors:

$$\lambda_p^+ = \left|\lambda_p\right| \cdot f_p^+ \quad \text{and} \quad \lambda_p^- = \left|\lambda_p\right| \cdot f_p^- \tag{20}$$

where index p is running over all eight eigenvalues of the system and f_p is the correction factor:

$$f_p^+ = max\left(0, \frac{\lambda_p}{\left|\lambda_p\right|}\right) + \frac{\phi_p}{2}\left(\left|\lambda_p\right|\frac{\Delta t}{\Delta x} - 1\right) \tag{21-a}$$

$$f_p^- = min\left(0, \frac{\lambda_p}{\left|\lambda_p\right|}\right) - \frac{\phi_p}{2}\left(\left|\lambda_p\right|\frac{\Delta t}{\Delta x} - 1\right) \tag{21-b}$$

The first term of the correction factors is the Godunov's first-order upwind discretisation, and the second term with the flux limiters ϕ_p is the second-order correction.

The eigensystem is evaluated from the Jacobian matrix where $\mathbf{C}^+_{j-1/2}$ corresponds to the waves that travel to the right with the positive characteristic velocities and $\mathbf{C}^-_{j+1/2}$ corresponds to the waves that travel to the left with the negative characteristic velocities. These matrices are correlated with Jacobian matrix $\mathbf{C}$ with the relation:

$$\mathbf{C}_{j-1/2} = \mathbf{C}_{(j-1)+1/2} = \mathbf{C}^+_{j-1/2} + \mathbf{C}^-_{j-1/2} \tag{22}$$

The Jacobian matrix shall be evaluated between two adjacent control volumes at points $j\pm 1/2$. A simple upwind average of the variables is used:

$$\mathbf{C}^+_{j-1/2} = \mathbf{C}^+\left(\frac{\vec{\psi}_j + \vec{\psi}_{j+1}}{2}\right) \tag{23}$$

Gallouet and Masella used this approach and showed that this type of averaging gives very accurate results for Euler equations [18]. This is actually the most important property of the proposed numerical method – the propagation velocity of the each of the eight acoustic waves that travel along the pipe can change with time and position. That means that the proposed numerical method enables introduction of the nonlinearities like pressure dependent density, two-phase flow, convective term, ovalization effects, variable geometry properties etc. This method is applicable for linear and nonlinear systems; the only required condition is hyperbolicity of the system.

The Courant-Friedrichs-Levy condition [17] is necessary and sufficient condition for the stability of the integration domain i.e. the explicit scheme is stable for time step Δt defined with condition:

$$\Delta t < CFL \cdot \frac{\Delta x}{max\left(\lambda_p\right)} \tag{24}$$

The recommended value for the CFL factor is approximately *0.9*.

3.2 Second-order correction

LeVeque described high-resolution method to solve the accuracy problem near discontinuous or sharp pressure and stress waves [17]. It is based on the characteristic upwind Godunov's method and includes a combination of the smearing first and the oscillatory second-order accurate discretisations. The eigenvalues in Eq. 20 are multiplied by correction factors defined in Eq. 21 where the first part of the correction factors is the first-order upwind discretisation, and the second part of the second-order discretisation is determined by the flux limiters ϕ_p, which "measure" the smoothness of the pressure or stress waves. If the waves are smooth, larger part of the second-order discretisation is used; otherwise larger part of the first-order discretisation is used. The high-resolution flux limiters ϕ_p are calculated using one of the following functions [17]:

$$\begin{aligned} &\phi_p = max\left(0, min\left(1, \theta_p\right)\right) \\ &\phi_p = \left|\theta_p\right| + \theta_p / (\left|\theta_p\right| + 1) \\ &\phi_p = max\left(0, min\left(2\theta_p, 1\right), min\left(\theta_p, 2\right)\right) \\ &\phi_p = max\left(0, min\left((1+\theta_p)/2, 2, 2\theta_p\right)\right) \end{aligned} \tag{25}$$

where θ_p measures "smoothness" of the modified characteristic variable in Eq. 14 near the point $j+1/2$. The ratio of the left and right gradients of the corresponding modified characteristic variable at the considered point is evaluated as:

$$\theta_{p,j+1/2} = \frac{\xi_{p,j+1-m} - \xi_{p,j-m}}{\xi_{p,j+1} - \xi_{p,j}} \tag{26}$$

where $m = \lambda_p / |\lambda_p|$ and $p = 1,..,8$. For a certain values of the flux limiters one can get some linear characteristic numerical schemes:

$$\begin{aligned} &\text{upwind (first order):} && \phi_p = 0 \\ &\text{Lax-Wendroff (second order):} && \phi_p = 1 \\ &\text{Beam-Warming (second order):} && \phi_p = \theta_p \end{aligned} \tag{27}$$

The transformation of the Eq. 19 back into the basic variables yields the following explicit finite difference scheme [16, 17]:

$$\begin{aligned} \vec{\psi}_j^{**} &= \vec{\psi}_j^{n} - \\ \mathbf{C}^{+}_{j-1/2}\left(\vec{\psi}_j^{*} - \vec{\psi}_{j-1}^{*}\right)\frac{\Delta t}{\Delta x} &- \mathbf{C}^{-}_{j+1/2}\left(\vec{\psi}_{j+1}^{*} - \vec{\psi}_{j}^{*}\right)\frac{\Delta t}{\Delta x} - \\ \mathbf{D}^{+}_{j-1/2}\vec{R}^{*}_{j-1/2}\Delta t &- \mathbf{D}^{-}_{j+1/2}\vec{R}^{*}_{j+1/2}\Delta t = 0 \end{aligned} \tag{28}$$

where $\mathbf{F}^+$ and $\mathbf{F}^-$ are diagonal matrices that contain correction factors defined in Eqs. 21:

$$\mathbf{D}^{+}_{j-1/2} = \left(\mathbf{L}\mathbf{F}^{+}\mathbf{L}^{-1}\right)_{j-1/2} \text{ and } \mathbf{D}^{-}_{j+1/2} = \left(\mathbf{L}\mathbf{F}^{-}\mathbf{L}^{-1}\right)_{j+1/2} \tag{29}$$

The iteration starts with: $\psi_j^* = \psi_j^n$.

Under certain conditions the source terms become stiff because the characteristic time scale of the source terms is much slower than the time step defined with the CFL condition in Eq. 24. Simple implicit iterative predictor-corrector numerical procedure is applied where the predicted variables in Eq. 28 are accepted and $\vec{\psi}_j^{n+1} = \vec{\psi}_j^{**}$ if:

$$\left|\frac{\vec{\psi}_j^{*} - \vec{\psi}_j^{**}}{\vec{\psi}_j^{*}}\right| \le \varepsilon \tag{30}$$

Else, the solutions are corrected/re-predicted with new iteration, using Eq. 28. Typically, there are less than two iterations needed, except in the presence of very sharp discontinuities in the source terms.

4 Rod impact experiment

4.1 The experimental setup

The rod impact experiment performed at University of Dundee by Tijsseling, Vardy and Fan [11] consisted of a single elbow piping system test setup (Fig. 3) hanging on long, thin, vertical steel wires, so it could move freely in a nearly horizontal plane. All geometry and state properties for the piping system, water and impact rod used in simulation are collected in Tab. 1.

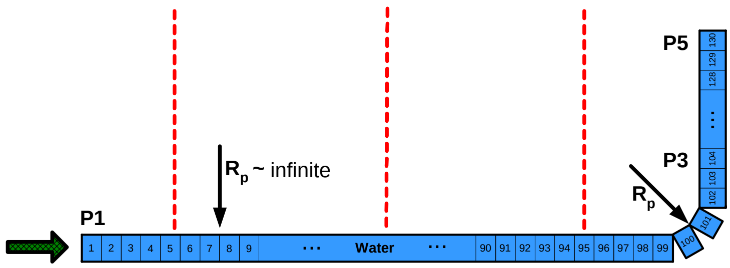

Fig. 3: Geometry and nodalization of the input model.

Tab. 1: Piping system, water and impact rod properties

Piping system	***Water***	***Impact rod***
L = 5.85 m (4.50m + 1.35m)	ρ_f = 999 kg/m^3	L_{rod} = 5.0 m
R = 0.02601 m	K = 2.14 GPa	R_{rod} = 0.02537 m
e = 0.003945 m	p = 20 bar	E_{rod} = 200 GPa
E = 168 GPa	v = 0 m/s	ρ_{rod} = 7985 kg/m^3
ρ_t = 7985 kg/m^3	T = 20 °C	$v_{0,rod}$ = 0.809 m/s
ν = 0.29		Y_{rod} = 80109.7 kg/s

Tab. 2: Position of the measuring equipment from the impact end

Label	***Position [m]***	***Volume [N]***	***Variable***	***Equipment***
P1	0.02	1	Pressure	Piezoelectric pressure transducer
P2	0.57	13	Axial velocity Axial strain	Laser-Doppler vibrometer Strain gauges (4 records)
P3	4.64	103	Pressure	Piezoelectric pressure transducer
P4	5.25	117	Axial strain	Strain gauges (4 records)
P5	5.85	130	Pressure	Piezoelectric pressure transducer

ISBN 978-3-901608-32-2

The longer section of the piping system was horizontal and the shorter section was vertical. The piping system was closed at both ends and filled with a pressurized tap water. Tijsseling et al. systematically performed several experiments with variable initial pressure, but only the case with sufficiently high initial pressure to prevent cavitation in the fluid was simulated. The stress waves in the pipe wall and pressure waves in the water were generated simultaneously by the axial impact of a solid steel rod on a free end of the horizontal part of the piping system. Fig. 3 shows the input model for simulation that consists of computational grid with *130 computational nodes* and has the corresponding centerline curvature radius at the elbow $R_p=0.085\ m$.

The piping system was extensively instrumented [11]. Table 2 shows summary of the instrumentation needed to obtain data used in the simulation. The axial force was not measured but it is related to the cross-sectional averaged axial strain and pressure:

$$N_x = \left(E\varepsilon_x + \nu \frac{R}{e} p \right) \tag{31}$$

The bending momentum is related to the top and bottom axial stresses:

$$M_z = \frac{EI_t}{2(R+e)} \left(\varepsilon_{x,1} + \varepsilon_{x,3} \right) \tag{32}$$

4.2 Results

Figures from 4 to 6 show comparison between the calculated and measured pressure and Fig. 7 shows calculated pressure surface on pipe length-time plane. The former figures show excellent agreement of the calculation with measurement, and the later figure clearly shows pressure history at all positions of the pipe. The pressure in the fluid is controlled by axial velocity of the pipe (Fig. 9). At the beginning of the transient, the pipe almost uniformly moves in direction of the impact rod. Due to the junction coupling at the impact end the pressure is very high and at the remote end the pressure is very low. The high and low pressure waves are added up in the middle. The situation turns at 5 milliseconds and the low pressure can be encountered at the impact end and high pressure at the remote end. Note that axial stress waves travel with speed of sound in steel that is approximately 3 times faster than speed of sound in fluid that is close to the characteristic traveling velocity of the pressure waves. Fig. 9 shows also that axial velocity in vertical part of the pipe is few times smaller that axial velocity in horizontal part of the pipe. Fig. 10 shows that maximal axial force is encountered at the beginning of the transient after the strike of the impact rod. Later on, the axial force oscillates around initial value. The bending momentum surface in Fig. 14 shows that maximal bending momentum (peaks) appears in the vicinity of the elbow (position $x=4,5\ m$).

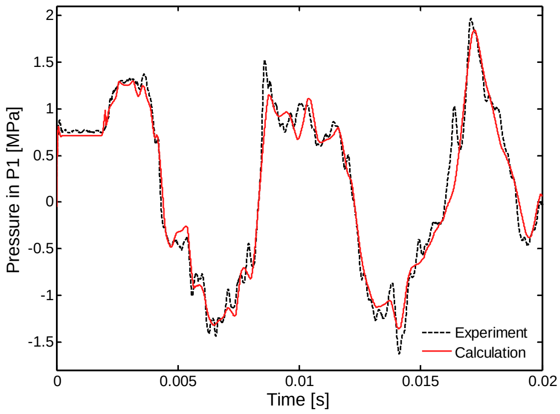

Fig. 4: Pressure history in P1.

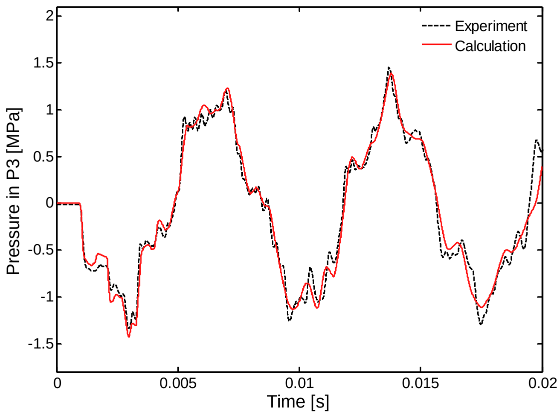

Fig. 5: Pressure history in P3.

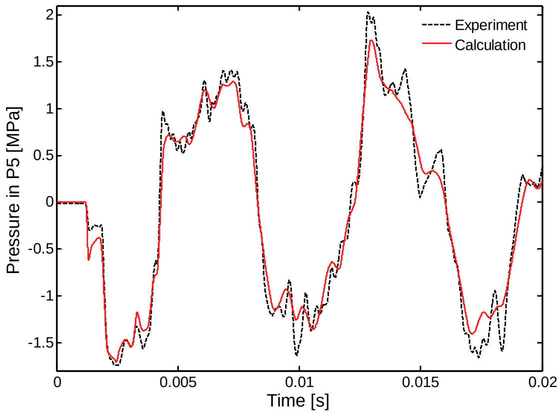

Fig. 6: Pressure history in P5.

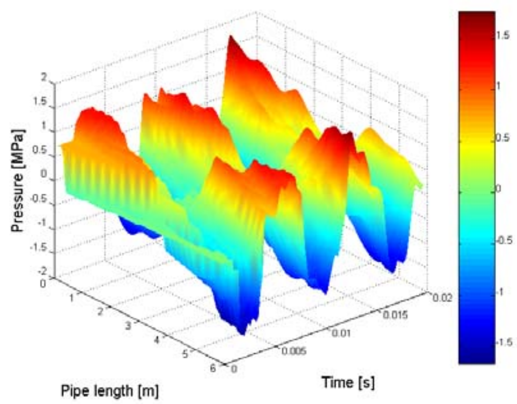

Fig. 7: Pressure in pipe.

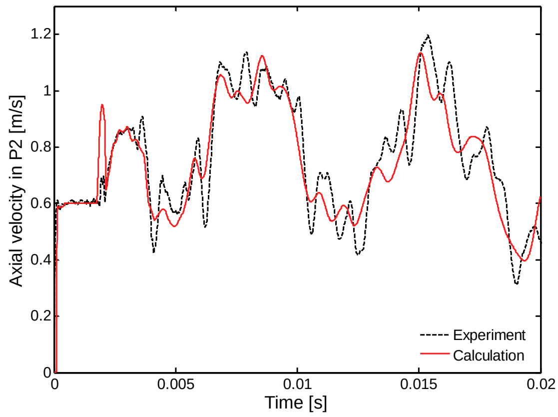

Fig. 8: Axial velocity history in P2.

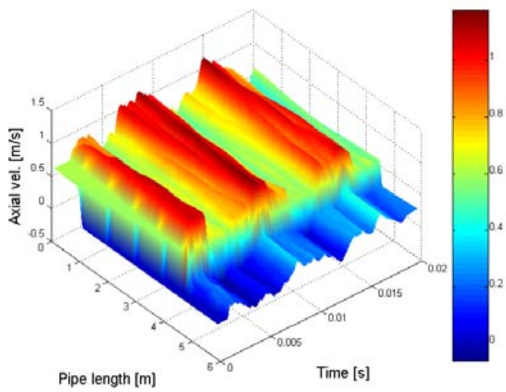

Fig. 9: Axial velocity in pipe.

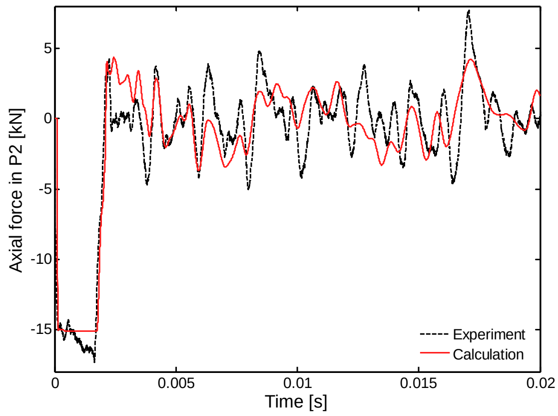

Fig. 10: Axial force history in P2.

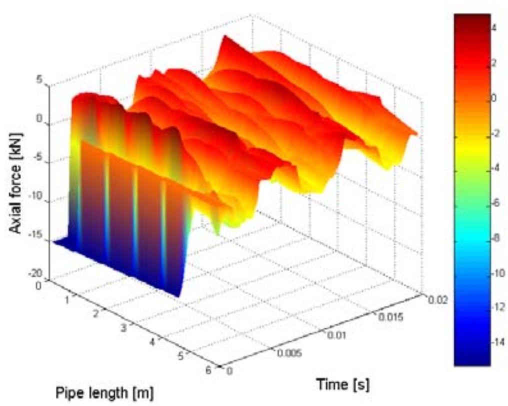

Fig. 11: Axial force in pipe.

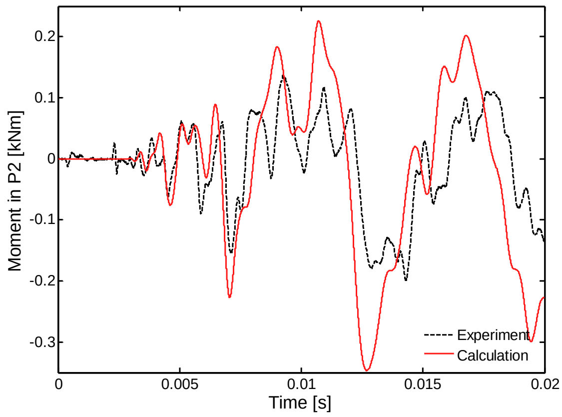

Fig. 12: Momentum history in P2.

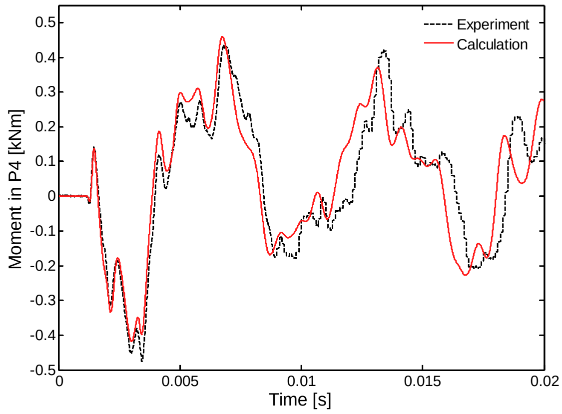

Fig. 13: Momentum history in P4.

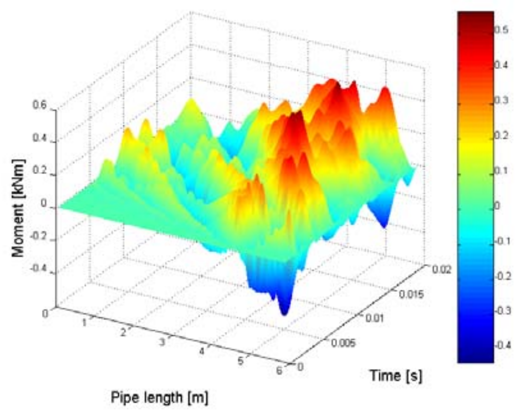

Fig. 14: Momentum in pipe.

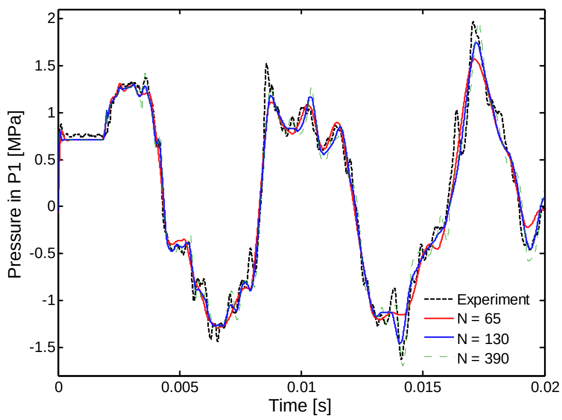

Fig. 15: Pressure history in P1, grid refinement.

ISBN 978-3-901608-32-2

The axial velocity, axial force and bending momentum at different positions along the pipe are compared to the measurement and the agreement between measurement and calculation is excellent especially in a view of complexity of the phenomena. Tijsseling et al. [11] and Lavooij and Tijsseling [2] who used similar mathematical system for description of the sharply connected straight sections and MOC numerical method obtained the same degree of agreement. The comparison validates and confirms the proposed model in the field of the considered FSI problems.

4.3 Grid refinement study

Fig. 15 shows grid refinement study. The results converge with grid refinement and computational effort penalties are very low and depend on number of computational volumes. The numerical scheme is explicit thus the time step is defined with standard Courant-Friedrichs-Levy condition (Eq. 24). For simulation of the first 20 milliseconds of the rod impact experiment (130 comp. nodes) less than 2 minutes on 3.0 GHz P IV processor are needed.

4.4 Nonlinear system of equations

Convective part in the fluid momentum balance equation is very small and it was thus initially neglected:

$$v\frac{\partial v}{\partial x} \ll 1 \quad \rightarrow \quad v\frac{\partial v}{\partial x} = 0 \qquad (33)$$

This term can be included into the fluid momentum equation to demonstrate the ability of the characteristic upwind numerical method to solve nonlinear hyperbolic systems. Figure 16 shows how the first four eigenvalues of the nonlinear system of equations varies with time and position (other four eigenvalues are not influenced by the convective term). The ability to simulate nonlinear systems or systems with variable material and geometry properties along piping system or parameters that are variable with time is very important property, which one can address as advantage of the characteristic upwind numerical scheme in comparison to conventionally used numerical methods. Figure 17 shows and confirms that the influence of the convection is actually negligible for the experiment considered in the present paper.

4.5 Von Mises stress

Von Mises stress is a scalar function of the components of the stress tensor that gives an appreciation of the overall magnitude of the tensor. In terms of a local coordinate system the Von Mises stress can be expressed as:

$$\sigma_v = \sqrt{\frac{1}{2}\left(\sigma_{xy}^2 + \sigma_{yz}^2 + \sigma_{zx}^2\right) + 3\left(\tau_{xy}^2 + \tau_{yz}^2 + \tau_{zx}^2\right)} \quad (34)$$

where (next page):

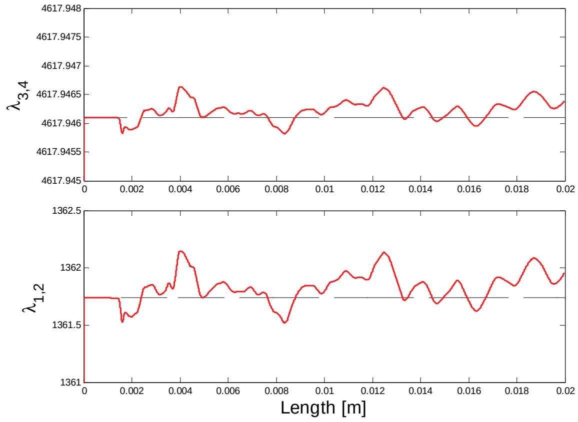

Figure 16: Eigenvalues history in point P4.

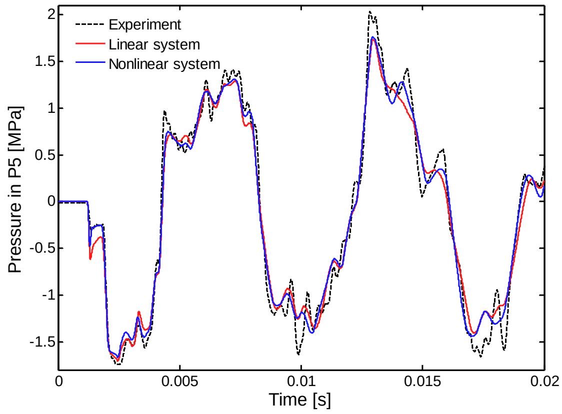

Figure 17: Pressure history in P5 – nonlinear system.

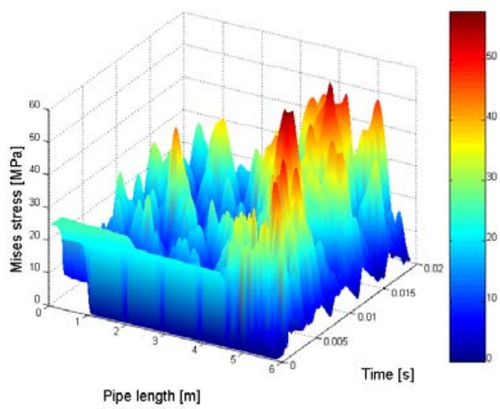

Figure 18: Mises stress in pipe – upper part

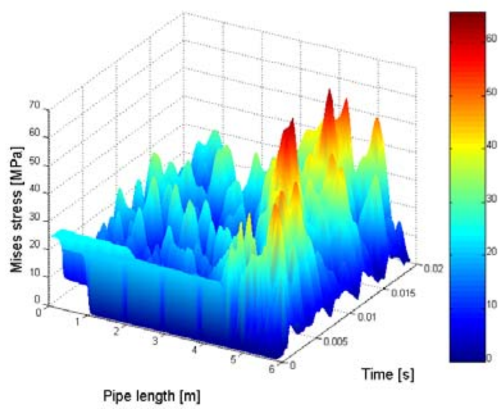

Figure 19: Mises stress in pipe – below part.

$$\sigma_{ij}^2 = \left(\sigma_i - \sigma_j\right)^2 \qquad \text{and} \qquad i, j = x, y, z \qquad (35)$$

Fig. 18 shows Mises stress in the top point of the pipe cross-section and Fig. 19 shows Mises stress in botom point of the pipe cross-section. These figures are very illustrative, because it is evident that critical section of the pipe with maximal load is section in vicinity of the elbow, further the maximal stresses are less than 60 MPa (typical yield stress for stainless steel is some 250 MPa), and duration of the maximal stresses is very short – pulsations.

5 Conclusions

The eight-equation system for description of the joint dynamics of the fluid and arbitrarily shaped piping structure was numerically solved with the second-order characteristic upwind numerical scheme. The most important advantages of the proposed model are efficiency, robustness, stability and accuracy. The proposed model enables advanced analyses of the fluid transients; the results can significantly improve experimental data due to high conformance between measurement and calculation; the results can also serve as very reliable tool for design of new piping systems. The weak points of the proposed model are limitation on plane piping systems and single-phase flow. The former limitation of the model can be avoided with trivial extension of the Timoshenko beam equation for out-of-plane direction and with inclusion of equations for torsional motion. The extension of the model to two-phase flow is an important issue and the model is under development.

Acknowledgements

The Ministry of Higher Education, Science and Technology of the Republic of Slovenia supported this work.

References

[1] A. S. Tijsseling, “Fluid-Structure Interaction in Liquid-Filled Pipe Systems: A Review“, Journal of Fluids and Structures, 10, pp. 109-146, 1996.

[2] Lavooij, C. S. W., Tijsseling, A. S., 1991, “Fluid-Structure Interaction in Liquid-Filled Piping Systems“, Journal of Fluids and Structures, 5, pp. 573-595.

[3] Casadei, F., Halleux, J. P., Sala, A., Chille, F., 2001, “Transient Fluid-Structure Interaction Algorithms for Large Industrial Applications“, Computer Methods in Applied Mechanics and Engineering, 190, pp. 3081-3110.

[4] Tiselj, I., Černe, G., Horvat, A., Gale, J., Parzer, I., Giot, M., Seynhaeve, J. M., Kucienska, B., Lemonnier, H., 2004, “WAHA3 Code Manual“, WAHALoads project deliverable D10, Ljubljana,

[5] Wylie, E. B., Streeter, V. L., 1978, Fluid Transients, McGraw - Hill International Book Company, New York.

[6] Païdoussis, M.P., , Fluid-Structure Interactions - Slender structures and axial flow, Volume 1 & 2, Academic Press, San Diego 1998, Elsevier Academic Press, London, 2004.

[7] Wiggert, D. C., 1986, “Coupled Transient Flow and Structural Motion in Liquid-Filled Piping Systems: A Survey”, Proc. of the ASME Pressure Vessels in Piping Conference, Paper 86-PVP-4.

[8] Wiggert, D. C., Tijsseling, A. S., 2001, “Fluid transients and fluid-structure interaction in flexible liquid-filled piping”, ASME Applied Mechanical Review, 54(5), pp. 455-481.

[9] Valentin, R. A., Phillips, J. W., Walker, J. S., 1979, “Reflection and Transmission of Fluid Transients at an Elbow”, Transactions of SMiRT5, Paper B 2-6.

[10] Skalak, R., 1956, “An Extension of the Theory of Waterhammer”, Trans. of the ASME, 78, pp. 105-116.

[11] Tijsseling, A. S., Vardy, A. E., Fan, D., 1996, “Fluid-Structure Interaction and Cavitation in Single-Elbow Pipe System”, Journal of Fluids and Structures, 10, pp. 395-420.

[12] Hu, C. K., Phillips, J. W., 1981,”Pulse Propagation in Fluid-Filled Elastic Curved Tubes”, ASME Journal of Pressure Vessel Technology, 103, pp. 43-49.

[13] De Jong, C. A. F., 1994, “Analysis of Pulsations and Vibrations in Fluid-Filled Pipe Systems”, PhD. Thesis, Eindhoven University of Technology, Department of Mechanical Engineering, Eindhoven, The Netherlands.

[14] Harvey, A. H., Peskin, A. P., Klein, S. A., 2004, “NIST Standard Reference Database 10,” NIST/ASME Steam properties, Ver. 2.21, US Department of Commerce.

[15] Taylor, S. T., Yau, S. C. B., 2003, Boundary control of a rotating Timoshenko beam, ANZIAM - Australian & New Zealand Industrial and Applied Mathematics Journal, 44 E: 143-184.

[16] Tiselj, I., Petelin, S., 1997, “Modelling of Two-Phase Flow with Second-Order Accurate Scheme”, Journal of computational physics, 136, pp. 503-521.

[17] Le Veque, R. J., 2002, Finite volume method for hyperbolic problems, Cambridge University Press, Cambridge.

[18] Gallouet, T., Massela, J. M., 1996, “A Rough Godunov Scheme”, C.R.A.S. Paris, 323, pp. 77-84.

